Simulation of deformation and fracture initiation during equal channel angular pressing of AZ31 magnesium alloy with covered tube casing

Eivani, A. R.; Mirghasemi, S. M.; Seyedein, S. H.; Zhou, J.; Jafarian, H. R.

DOI
10.1016/j.jmrt.2021.03.096

Publication date
2021

Document Version
Final published version

Published in
Journal of Materials Research and Technology

Citation (APA)
Eivani, A. R., Mirghasemi, S. M., Seyedein, S. H., Zhou, J., & Jafarian, H. R. (2021). Simulation of deformation and fracture initiation during equal channel angular pressing of AZ31 magnesium alloy with covered tube casing. *Journal of Materials Research and Technology*, *12*, 1913-1923. https://doi.org/10.1016/j.jmrt.2021.03.096

Available online at www.sciencedirect.com

jmr&t Journal of Materials Research and Technology

journal homepage: www.elsevier.com/locate/jmrt

Original Article

Simulation of deformation and fracture initiation during equal channel angular pressing of AZ31 magnesium alloy with covered tube casing

A.R. Eivani [a,*], S.M. Mirghasemi [a], S.H. Seyedein [a], J. Zhou [b], H.R. Jafarian [a]

[a] School of Metallurgy and Materials Engineering, Iran University of Science and Technology, Tehran, Iran
[b] Department of Biomechanical Engineering, Delft University of Technology, Mekelweg 2, 2628 CD, Delft, the Netherlands

ARTICLE INFO

Article history:
Received 25 November 2020
Accepted 23 March 2021
Available online 31 March 2021

Keywords:
Finite element simulation
Equal channel angular pressing
Fracture
Magnesium
Workability

ABSTRACT

The present research was aimed at lowering the deformation temperature by applying cover tube casing (CTC) to AZ31 magnesium alloy samples subjected to equal channel angular pressing (ECAP) without triggering surface defects and/or fracture. The Cockcroft-Latham (C & L) fracture model was incorporated into finite element simulation and the critical values for a fracture to occur were determined. The fracture was predicted for the samples deformed at 150, 175, and 200 °C without CTC and with CTC having thicknesses of 1 and 4 mm. The predictions of the model were verified with experimental data. It was found that the workability of AZ31 increased with increasing CTC thickness, as a result of a reduction in the maximum principal stress at the top surface, a uniform distribution of strains, and an increase in the critical damage. In practice, the use of CTC led to the possibility of a reduction in deformation temperature by 25 °C. A sound product with a homogeneous grain structure and a mean grain size of 11 μm was achieved at 175 °C. Thus, the ECAP working window for the alloy was enlarged with accompanying benefits in energy consumption, tooling life, and manufacturing costs.

1. Introduction

In traditional metallurgy, grain refinement is known as a method for improving the mechanical properties of structural materials, e.g., strength, ductility, and fatigue resistance. This may be considered as the main motivation for the development of severe plastic deformation (SPD) techniques [1]. Ultrafine grained (UFG) metals and alloys with significantly improved properties have been achieved by SPD processing on many different metallic materials, e.g., steels [2,3], aluminum and alloys [4–8], magnesium and alloys [8], and copper and alloys [9].

* Corresponding author.
E-mail address: aeivani@iust.ac.ir (A.R. Eivani).
https://doi.org/10.1016/j.jmrt.2021.03.096

Being well known for high specific strength, magnesium has been considered to be a promising material for structural parts where lightweight is desired, for example, for automotive parts. However, the use of magnesium products is largely restricted to cast products, although wrought products normally have higher mechanical performance and thus are more suitable for load-bearing applications. One of the major barriers to the widespread use of wrought magnesium products is the poor workability of magnesium [10] due to its hexagonal close-packed (HCP) crystal structure [11] with a limited number of independent slip systems operating at room temperature [12]. As a result, well-established bulk forming processes, such as extrusion, rolling, and forging, cannot be applied, unless the working temperature is raised above 225 °C, which increases equipment costs, energy costs, and manufacturing costs as a whole.

For wrought products, alloying of magnesium is often desired for the sake of mechanical properties and corrosion resistance, but it may also be used as a strategy to raise the workability of magnesium through modifying its deformation texture [13], or introducing a more deformable phase with a body-centered cubic (BCC) crystal structure [14], or refining its grain structure. The addition of aluminum to magnesium, for example, improves the strength and corrosion resistance of magnesium [15], also results in grain refinement, and increases its ductility. However, aluminum is a weak nucleant for magnesium grains and thus can only marginally reduce hot tearing susceptibility. The fundamental problem of poor workability of magnesium at temperatures below 225 °C remains largely unchanged. As a consequence, Mg–Al–Zn alloys still belong to a group of magnesium alloys with poor workability and have serious limitations for bulk forming processes involving large strains, such as severe plastic deformation (SPD) which serves as an effective means to achieve desirable grain refinement and mechanical properties [16].

SPD processing of Mg–Al–Zn alloys requires careful consideration of all process parameters, basically temperature, strain, and strain rate. An effective approach to broadening the applicable process parameters is to increase the temperature [17], thereby allowing more slip systems to operate, which are otherwise inactive at room temperature [18]. When the deformation temperature is increased, the strain rate plays an important role in determining the deformation behavior and the as-deformed microstructure. Therefore, it needs to be precisely controlled [19]. Kang et al. [20] investigated the SPD of the AZ31 alloy using equal channel angular pressing (ECAP) and found that at temperatures below 150 °C, all samples failed during ECAP. At temperatures higher than 200 °C, however, sound samples could be obtained at low strain rates. With deformation temperature increased to 250 °C, samples could be readily deformed over a wider range of strain rates. Similar results were obtained by Lapvok [21] and Figueiredo et al. [22]. The main reason behind these findings is that during SPD large, cumulative plastic strains are imposed on the material, which results in significant increases in dislocation density and grain refinement [1,23,24]. When deformation temperature is raised, dynamic or semi-dynamic recovery and recrystallization are activated, leading to dislocation annihilation, subgrain formation, and even recrystallization and grain growth, which undermines the results desired to achieve by applying SPD [25]. Therefore, it is a challenge to increase the workability of Mg–Al–Zn alloys and at the same time lower the deformation temperature for ECAP. Several strategies have been explored, such as tight control of deformation temperature and strain rate [20–22], application of backpressure [21,26,27], and change of die design [28–30]. As an alternative method to improve workability during ECAP, covered tube casing (CTC) has recently been proposed [31]; a copper tube on an aluminum sample resulted in improved strain distribution inside the aluminum sample [31]. Jahed et al. [32] investigated the effect of CTC on the fracture of the AM30 magnesium alloy at elevated temperatures of 200, 250, and 275 °C and confirmed improved workability. However, no attempts were made to lower the deformation temperature to the range where cracking or facture has a much stronger tendency to occur.

Over the temperature range below the critical temperature of 225 °C, the interplay between deformation temperature, strain, and strain rate becomes more important in determining the deformation responses, dynamic restoration mechanism, and failure mechanisms of Mg–Al–Zn alloys. The ECAP process parameters are further compounded by CTC thickness that determines the strain homogeneity and occurrence of fracture at a given deformation condition. In this regard, fracture models and deformation analysis using the finite elements (FE) method are of great help, as their combination is capable of predicting fracture at various processing conditions, before experimental research. Fracture models, such as the Cockcroft-Latham (C & L) model, consider material failure as a function of processing parameters, such as stress, strain, strain rate, and temperature. A fracture occurs when these parameters or a relationship containing these parameters exceeds a critical value [33]. The C & L model is one of the most widely used fracture models, which uses the maximum principal stress for the calculation of damage in a cumulative mode [34]. Due to some discrepancies observed between the predictions of the C & L model and the experimental results [22], normalized C & L criteria were proposed, in which the effect of the hydrostatic stress was included. However, the authors of the present communication demonstrated that the C & L model can more precisely predict fracture during ECAP processing of the AZ31 at room temperature than normalized C & L [35]. Besides, other fracture models, such as the stress ratio criterion [36], have been used for the prediction of fracture during ECAP at room temperature. To the best knowledge of the authors, there have been few attempts to predict the fracture of magnesium alloys during ECAP at moderately elevated temperatures.

The effect of the ECAP on the evolution of microstructure and mechanical properties of magnesium alloys, e.g., AZ31 has been thoroughly studied [8,15,37–39] and is not covered in this investigation. The current paper is focused on the prediction of fracture during ECAP of AZ31 alloy aimed at further improving the processing route of the AZ31 magnesium alloy. Because ECAP is used to apply extremely high amounts of deformation to refine the grain structure of metallic materials and achieve UFG structure or nano grained alloys, the deformation temperature should be kept below the recrystallization temperature. For most metals and alloys, SPD is

conducted at room temperature. However, room temperature deformation of magnesium alloys is not practical which is due to poor workability [10]. Therefore, magnesium alloys are mostly deformed at 200 °C or higher which is likely to result in dynamic recrystallization and reduced achievements by SPD. At lower temperatures, no recrystallization is expected, but fracture may occur. To optimize the processing route, C & L fracture model is incorporated into a FEM simulation of ECAP of AZ31 at moderately elevated temperatures. The effect of CTC on lowering applicable deformation temperature, improving the workability of the alloy, and refining the as-deformed grain structure is another aim of the current paper. The deformation temperature could be reduced by the CTC approach which is explained by the developed fracture model. The microstructures of the samples are investigated to demonstrate the importance of reducing deformation temperature on grain refinement.

2. Experimental procedure

The chemical composition of the AZ31 magnesium alloy used in this investigation was determined using optical emission spectroscopy according to ASTM B954-15 and is shown in Table 1. Hot extruded rods with a diameter of 48 mm were heated in an open atmosphere electrical resistance furnace at 400 °C for 24 h and then quenched in water [40]. This heat treatment was performed to eliminate intermetallic compounds, mostly the β-$Mg_{17}Al_{12}$ phase, from the matrix [41]. The samples were held at room temperature for 48 h before ECAP.

For ECAP processing, a die made of the H13 tool steel with two channels intersecting at 90° and an outer curved corner of 22° was used. The diameter of the channels was 16.05 mm. The whole die and sample set-up were heated using 4 heating plates surrounding the die to desired temperatures of deformation mentioned in Table 2. The temperature inside the die at a distance of 10 mm from the intersection of the two channels was measured using a thermocouple with an accuracy of ±5 °C. The die was heated to the desired temperature first. Then, the sample was inserted into the entry channel, and ECAP was performed after 10 min holding. MoS_2 grease was used for lubrication. For pressing, a 1 MN hydraulic press at a ram speed of 1.3 mm/s was used.

Table 1 – Chemical composition of the alloy used in this investigation (wt.%).

Mg	Al	Zn	Mn	Other
Base	2.5	0.76	0.26	<0.3

Table 2 – Labels of the samples used in this investigation.

Thickness of Cu tubes (mm)	Temperature (°C)			
	25	150	175	200
0	25–0	150–0	175–0	200–0
1	–	150–1	175–1	200–1
4	–	150–4	175–4	200–4

To investigate the effect of CTC on the workability and fracture occurrence of AZ31, pure copper tubes (purity: 99.9%) with thicknesses of 1 and 4 mm were used. The outer diameter of the tubes was 16 mm and the inner diameters were 8 and 14 mm, as listed in Table 2. Sample without CTC was subjected to the same ECAP processing for comparison purposes.

A Huvitz optical microscope was used to determine the effect of ECAP processing on the evolution of grain structure. The observation was made on the longitudinal section of the deformed samples. After cutting, grinding, and polishing, samples were chemically etched using a solution composed of 1 mLl HNO_3, 1 mL CH_3COOH, and 1 g $C_2H_2O_4$ in 150 mL deionized water. The grain sizes of the samples before and after ECAP were determined by using the linear intercept method.

3. Fracture model and FE simulation

To reveal deformation parameters and damage inside the AZ31 alloy sample during ECAP, a Deform 3D software package was used. To introduce the material behavior into the simulations of ECAP, the material model of AZ31 available in the Deform 3D package was used. The simulations were performed at 150, 175, and 200 °C. The shear friction model was applied to represent contact conditions between the workpiece and the FSP tool. By taking advantage of the symmetry of the ECAP setup, one half of the sample with 20,000 non-uniform tetrahedral elements and minimum and maximum sizes of 1 and 2 mm was modeled. Remeshing was performed in the areas where deformation exceeded a predetermined distortion value of 30%. During the simulations of ECAP of the samples with CTC, an existing material model of pure copper in the software package was used. 15,000 and 18,000 tetrahedral elements were used for CTC with thicknesses of 1 and 4 mm, respectively. The same re-meshing criterion and symmetrical conditions as those used for ECAP without CTC were applied. Both the sample and CTC were simplified as plastic materials with their elastic behavior ignored.

A rigid ram with a diameter of 16 mm and length of 160 mm was meshed with 20,000 elements and minimum and maximum sizes of 1.2 and 2.1 mm. As the whole die was heated up to the deformation temperature, and considering the significantly higher volume of the die to the deforming sample, the temperature of the die was considered to stay unchanged during the simulation. As the ram is not heated up, heat transfer to the ram was incorporated into the model. Thermal characteristics of the workpiece and tool which are used in the simulation are presented in Table 3.

Ram speed was the same as that applied in the experiments, i.e., 1.3 mm/s. The die was also considered to be rigid

Table 3 – Thermal and friction characteristics used in this investigation.

Property	AZ31 alloy	H13
Thermal conductivity (W/mK)	84	24.5
Heat capacity (kJ/m3K)	2096	4500
Coefficient of friction	0.4	–

and modeled to be the same as the experimental setup with an intersection angle of 90° and an outer curved corner of 22°. The simulation was performed for 500 steps with 0.2 mm ram displacement at each step. The distributions of strains, strain rates, and temperatures were reported as the outputs of the simulations.

The C & L fracture criterion, as expressed in Eq. (1), was used to predict the occurrence of fracture during ECAP, when the cumulative damage exceeded a critical value, C. The critical damage value is usually determined from tensile tests. The damage of a deforming sample is calculated as a cumulative parameter.

$$c = \int_0^{\varepsilon_f} \sigma_1 \, d\varepsilon_p \tag{1}$$

where σ_1 is the maximum principal stress, ε_p the equivalent strain, and ε_f the equivalent strain at which fracture occurs.

4. Results and discussion

4.1. *Estimation of the critical value for the C & L fracture model*

As previously shown [35], the critical value in the C & L criterion can be estimated by calculating the area under the stress–strain curve obtained from tensile test at room temperature. With changes in temperature and strain rate applied in tensile tests, the area under the stress–strain curve changes accordingly and as a result, the critical value changes. Therefore, in one single ECAP deformation process, the critical value and the probability of fracture may be different for the deformation conducted locally at different temperatures and strain rates. Besides, when deformation is conducted at an elevated temperature, inhomogeneous distributions of temperatures and strain rates inevitably occur. Fig. 1 shows the distributions of temperatures and strain rates in a sample deformed at 150 °C without CTC, as an example. It can be seen that the sample has different values of temperature and strain rate throughout the longitudinal section. This will cause varied histories of strain rate and temperature in different regions on the longitudinal section of the sample. It is thus impossible to choose one specific temperature or strain rate to be applied in the tensile test to calculate the critical value.

Hypothetical stress–strain curves at different temperatures and strain rates during deformation are shown in Fig. 2. A critical value at a specific spot inside the ECAP sample can be obtained by calculating the sum of S1, S2, S3, and S4, as the area underneath stress–strain curves of the samples at different conditions. Any specific spot inside the sample may experience many combinations of temperatures and strain rates during ECAP. As a result, the calculation of the critical values by estimating the true deformation history requires the availability of a large number of data, which is not practical.

A way around the problem in the present research is to perform the simulations of ECAP without implementing the fracture criterion first to calculate the cumulative damage in different regions of the deforming sample. At this step, a fracture is not predicted, because no fracture criterion is activated. From experimental observations and those reported in the literature [20–22], it is understood that Mg alloys including AZ31 cannot withstand deformation in ECAP at room temperature or even at temperatures below 200 °C. Under these conditions, surface cracks form in the upper region of the sample during ECAP, while the bottom and middle regions remain intact [20–22]. One may thus infer that the cumulative damage in the upper region, predicted by the simulation, is equal to or larger than the critical value. Besides, the predicted damage in the other regions, even in the most damaged area, is below the critical value simply because no fracture is observed in these regions. Therefore, the value of damage in the highly damaged area but still with damage less than the upper region is assumed to be a critical value. This way of estimating the critical value provides a certain factor of safety for future predictions, which makes the approach practically viable.

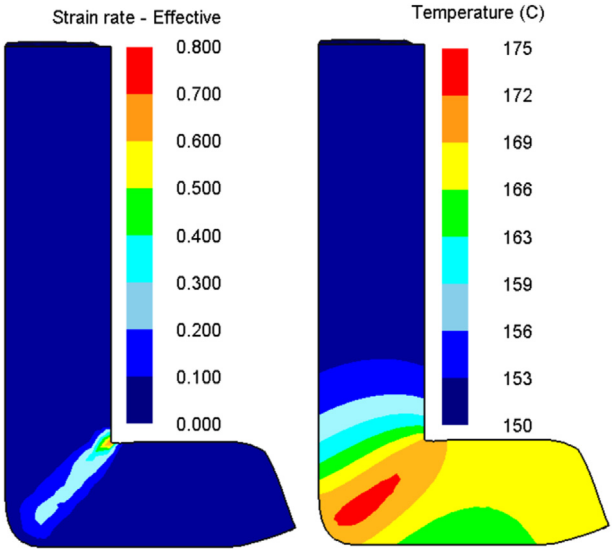

Fig. 1 – FEM predicted distributions of the effective strain rates and temperatures in a sample deformed at 150 °C.

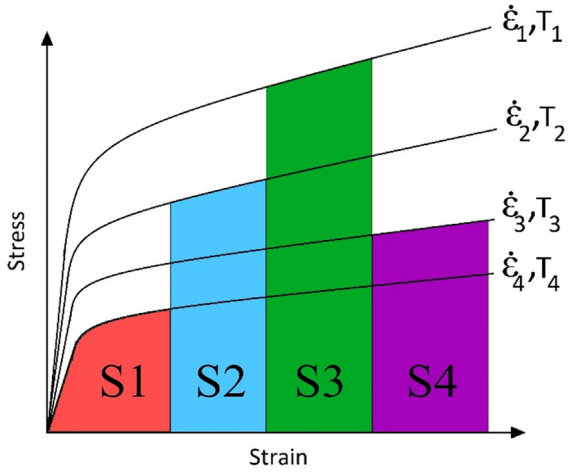

Fig. 2 – Hypothetical variations in strain rate and temperature at one specific spot in a deforming sample during ECAP.

The predictions of the cumulative damage in the samples deformed at 150, 175, and 200 °C are shown in Fig. 3. As discussed earlier, the maximum damage occurs in the upper region of the deformed samples. The values of the cumulative damage in this region were 20, 25, and 30 MPa for the samples deformed at 150, 175, and 200 °C, respectively. It should be noted that the values to be used in the simulations with the implementation of the fracture criterion are tentative and may be subjected to change or correction if the predictions do not agree with experimental results.

4.2. *Simulation of ECAP with the fracture criterion implemented*

The results obtained from the simulations of ECAP of the AZ31 alloy deformed at 150, 175, and 200 °C with CTC thicknesses of 0, 1, and 4 mm are shown in Fig. 4. At 150 °C, fracture occurs in all samples from the top surface, as indicated by the red color (Fig. 4a). Without CTC, fracture occurs through the thickness of the sample. With CTC, however, fracture proceeds only halfway through the thickness. The application of CTC results in reductions in cumulative damage and thus fracture in the sample.

In the case of the sample deformed at 175 °C (Fig. 4 b), the sample without CTC appears to be the same as the one deformed at 150 °C. However, no fracture is observable in the sample with CTC. Minor signs of damage appear at the surface of the sample with 1 mm thick CTC, but no damage is observed in the sample with 4 mm thick CTC. Damage and thus fracture reduce with increasing CTC thickness. For the sample deformed at 200 °C (Fig. 4c), the fracture does not appear in any of the samples; with or without CTC, a sound deformed product is achieved, although minor signs of damage are observed at the surface of the sample without CTC. It confirms that fracture in the ECAPed samples reduces with increasing CTC thickness.

To quantify the extent of damage, the variation in the C & L damage on the longitudinal section of the sample was extracted (Fig. 4). The damage is presented along with the distance from the upper region to the bottom region of the sample, as illustrated by the black rectangular box in the figure. For all the samples, the maximum damage occurs at the top surface, the damage lessens towards the center and increased again towards the bottom surface. This is consistent with the experimental observation that fracture initiates on the top surface [20–22]. In Fig. 4, a dashed line is drawn to indicate a critical value of damage, above which the cumulative damage is larger than the critical value and fracture may occur in the sample or part of the sample. The value of critical damage increases with increasing deformation temperature. It can be seen in Fig. 4a that the damage at the top surface exceeds the critical value at 150 °C, with or without CTC. In addition, the damage is very close to the critical value even in the core regions, indicating the likelihood of fracture or severe cracking inside the deformed sample. With deformation temperature increased to 175 °C, the damage of the samples with CTC is reduced and becomes lower than the critical value. However, for the sample without CTC, the damage still exceeds the critical value up to almost 3 mm under the top surface. For the samples deformed at 200 °C, the damage is all below the critical value, with or without CTC.

To ascertain the predictions of fracture, the maximum principal stress and the effective strain in the black rectangular box indicated in Fig. 4, were extracted (Fig. 5). As can be seen in Fig. 5a, the maximum principal stress reduces from the top surface towards the bottom. The trend is the same for all the samples. The slope of the reduction is the highest at 150 °C. The variation of the effective strain on the cross-section of the sample follows the same pattern for the samples with or without CTC at 150 °C and without CTC at 175 °C only. Indeed, the maximum values of the effective strain

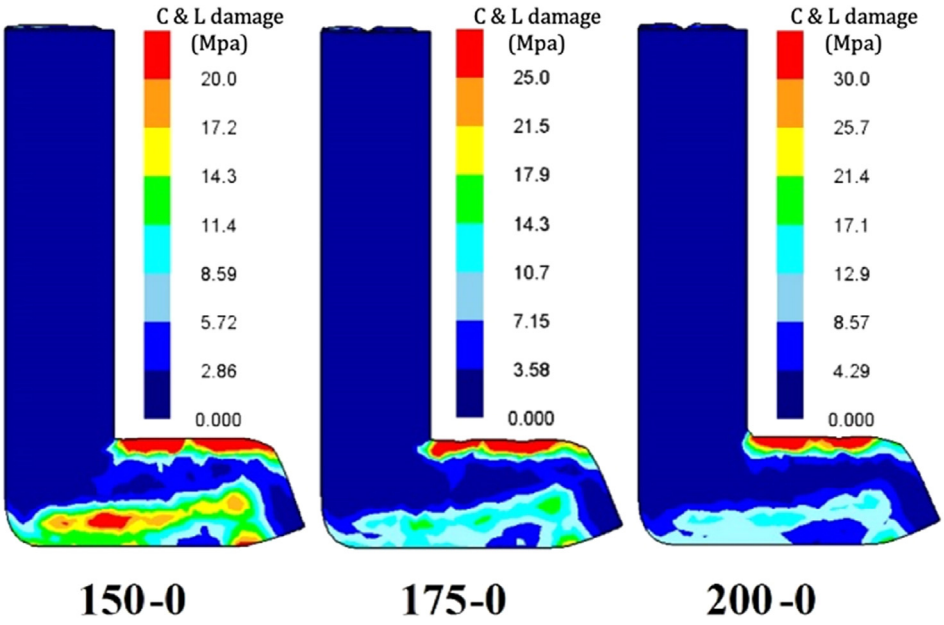

Fig. 3 – Results of preliminary simulations showing the extent of predicted damage during ECAP at different temperatures.

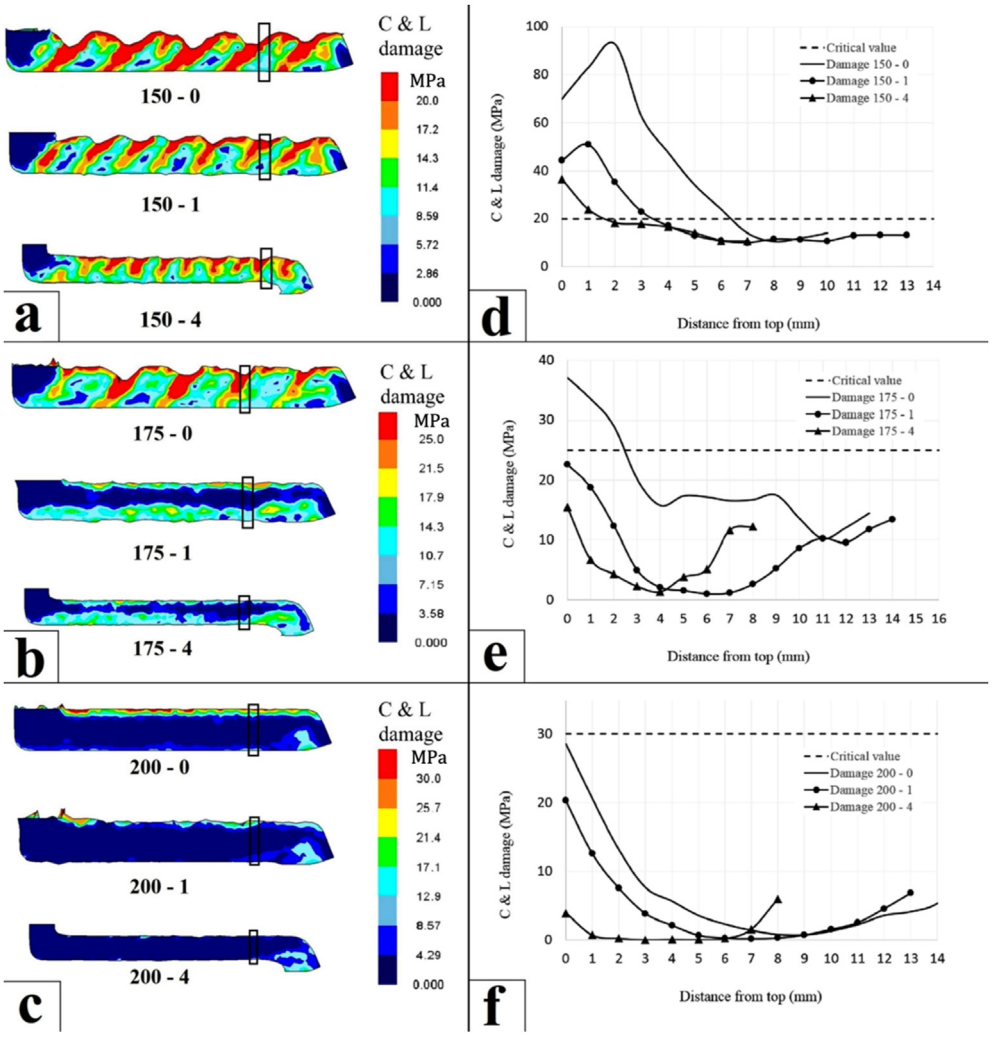

Fig. 4 – Predictions from the simulations showing (a), (b), and (c) fractured samples and the distributions of damage values on the longitudinal section and (d), (e), and (f) the distribution of the C & L damage values through the thickness of the samples with 0, 1 and 4 mm thick CTC and deformed at (a) and (d) 150, (b) and (e) 175 and (c) and (f) 200 °C.

occur at the surface of the samples. According to the C & L fracture criterion, high cumulative damage is an outcome of high levels of the principal stresses and effective strains. In the other regions of the samples, with increasing distance towards the bottom, both values of the effective strain and maximum principal stress and, therefore, the damage reduction. For the samples deformed at 175 °C with CTC and those deformed at 200 °C, however, the effective strains from the top to the bottom remain at a low level, although the maximum principal stress is the highest at the top surface and reduces towards the bottom. It seems to indicate the effective strain to be a more important parameter to decide the occurrence of fracture. Variations in maximum principal stress and effective strain through-thickness reduce with using CTC and increasing CTC thickness. Indeed, deformation becomes more uniform with the application of CTC and increasing CTC thickness. This results in reduced localization of deformation and accumulative damage which are required for initiation of fracture. It should be added that the highest values of maximum principal stress and effective strain, which occur at the top surface of the sample, are reduced by the application of CTC and increasing CTC thickness. According to the formulation of C & L fracture criterion in Eq. (1), reduced maximum principal stress results in lower values of accumulative damage to acquire the critical value and initiate fracture. Reduced value of effective strain which is achieved at the surface of the CTC-deformed samples may result in the same consequence and postponed fracture initiation.

4.3. *Verification of the predicted results*

To verify the predictions made from the simulations, AZ31 samples were deformed at the same conditions as those used in the simulations. The images of the deformed samples are presented in Fig. 6. Fracture indeed occurred in all samples deformed at 150 °C. A magnified image of a fractured sample with 4 mm thick CTC and deformed at 150 °C, showing the

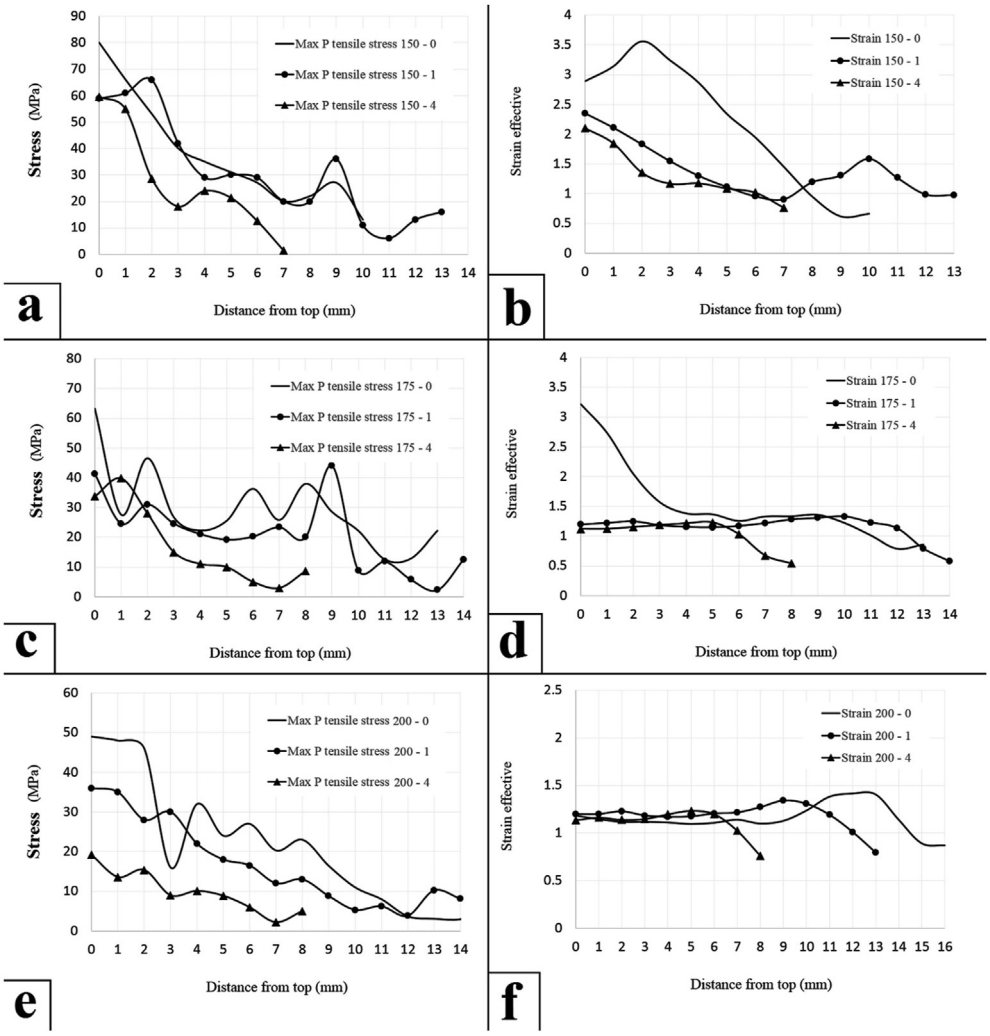

Fig. 5 – Distributions of (a), (c) and (e) the maximum principal stresses and (b), (d), and (f) the effective strains through the thickness of the samples with 0, 1, and 4 mm thick CTC and deformed at (a) and (b) 150, (c) and (d) 175 and (e) and (f) 200°.

extent of damage, is presented in Fig. 7a. With temperature increased to 175 °C, the damage reduced, and in the sample with 1 mm thick CTC, no fracture was observed. In addition, sound samples were achieved, when they were deformed at 200 °C. However, it should be noted that, as shown in Fig. 7b, surface cracks formed in the sample without CTC and deformed at 200 °C. Such surface cracks were however not observed in the sample with 1 mm thick CTC and deformed at

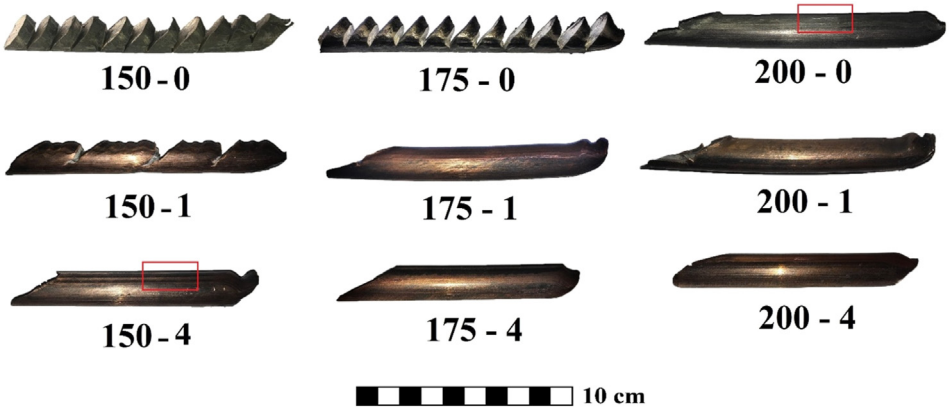

Fig. 6 – Samples with CTC of different thicknesses, deformed at different temperatures.

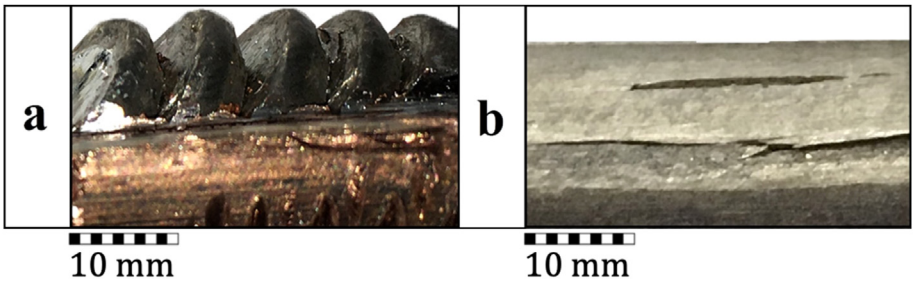

Fig. 7 – Fracture in (a) the sample with 1 mm thick CTC and deformed at 175 °C and (b) surface cracks in the sample without CTC and deformed at 200 °C.

175 °C. These results are all in good agreement with the predictions from the simulations, indicating that the application of CTC indeed helps lower the deformation temperature by 25 °C and yet a sound product is achievable. A reduction in deformation temperature leads to reductions in energy consumption, die damage, and manufacturing costs. In addition, as will be shown later, it benefits the microstructure that is of great importance, because it is one of the main reasons for applying SPD.

4.4. *Evolution of microstructure*

The results from the simulations and experiments presented earlier clearly show that deformation temperature may be lowered by 25 °C if CTC is utilized in the ECAP of the AZ31 alloy. It is important to know the effect of such a reduction in deformation temperature on the as-deformed microstructure. In Fig. 8, the grain structure of the sample with 1 mm thick CTC and deformed at 175 °C is compared to that of the sample without CTC and deformed at 200 °C, relative to the microstructure of the AZ31 alloy before ECAP. It can be seen that the initial microstructure of the alloy is composed of circular, equiaxed grains with a mean grain size of 39 μm and without any preferred orientation. By contrast, the sample deformed at 175 °C has elongated coarse grains oriented in the deformation direction (the white arrow) and also fine recrystallized grains mostly at the boundaries of the initial grains (Fig. 8b). The fraction of recrystallized grains is below 10%. The mean grain size of this sample is 11 μm. This demonstrates the effectiveness of ECAP processing in grain refinement. The sample deformed at 200 °C without CTC (Fig. 8c) has fine, recrystallized grains and also coarse, deformed grains. The fraction of recrystallized grains is above 30% and the mean grain size is 12 μm, which does not differ markedly from that of the sample with 1 mm thick CTC and deformed at 175 °C. Such a small difference may be considered to be within an error margin and the grain structures may be considered to be essentially the same. This is because the recrystallized grain structure is dynamically formed without much grain growth and the mean grain size is thus independent of the deformation temperature [25].

The distributions of the diameter of the grains on the plane of measurement are presented in Fig. 9. The sample before ECAP has a broad distribution of grain sizes, ranging from 10 to 80 μm. When the material is deformed, grain sizes reduce and limit themselves to values less than 50 μm, as a result of the refinement of the initially coarse grains. The grains at the surface region have more uniform sizes than those in the other regions. After ECAP, the number density of fine grains is significantly increased in both of the samples. This is obviously because of the formation of fine recrystallized grains. When the area fractions of grains over different size ranges are considered, the grain structure of the sample with 1 mm thick CTC and deformed at 175 °C is more homogeneous than that of the sample without CTC and deformed at 200 °C. Therefore, one may conclude that the reduction in deformation temperature as a result of the use of CTC leads to a more uniform microstructure after ECAP.

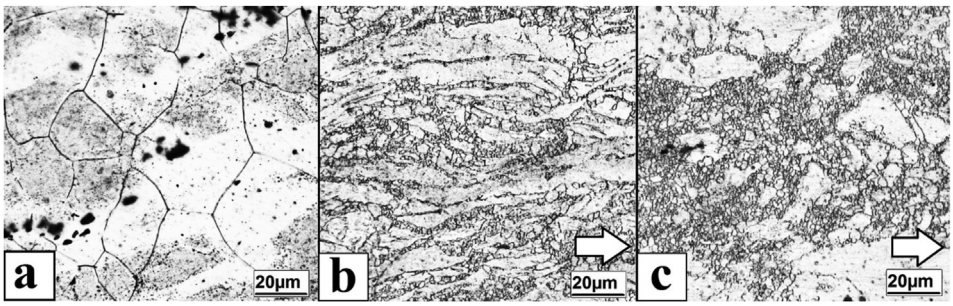

Fig. 8 – Grain structures of (a) the sample before ECAP, (b) the sample with 1 mm thick CTC and deformed at 175 °C, and (c) the sample without CTC and deformed at 200 °C.

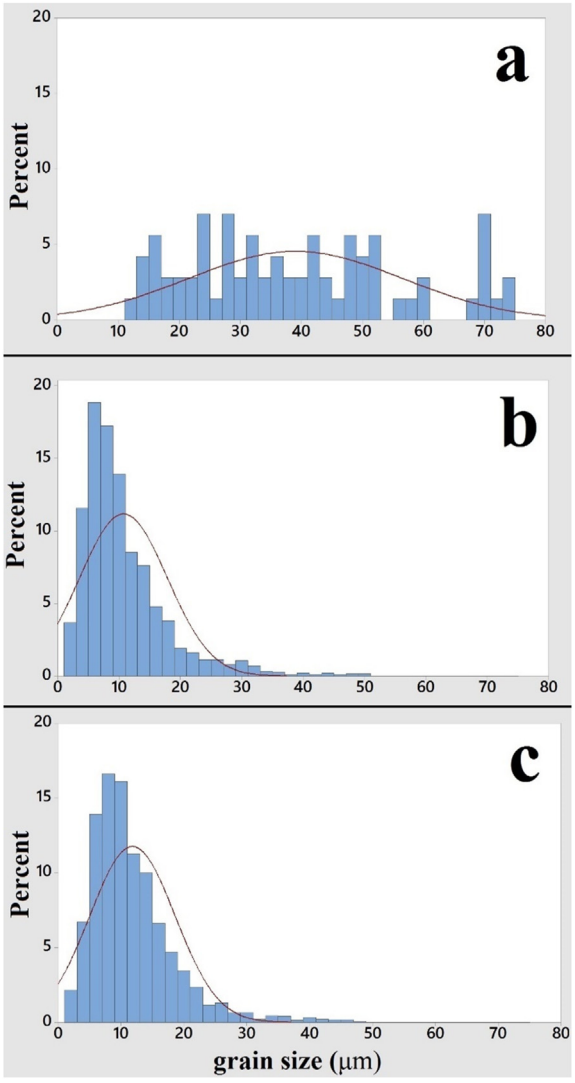

Fig. 9 – Distributions of grain sizes of (a) the sample before ECAP, (b) the sample with 1 mm thick CTC and deformed at 175 °C, and (c) the sample without CTC and deformed at 200 °C.

5. Conclusions

In this investigation, the effect of CTC on the workability, damage, and fracture of AZ31 samples during equal channel angular pressing (ECAP) was investigated employing FE simulation and validated by experiments. Accumulative damage values in deformed samples were calculated using the C & L criterion incorporated into the DEFORM FE simulation program. In addition, the effect of lowered deformation temperature on the grain structure was investigated. The following conclusions have been drawn.

(1) The fracture occurs at the top surface of the sample during ECAP when the cumulative damage exceeds a critical value. This is because the parameters determining the occurrence of fracture, i.e., the maximum principal stress and the effective strain, are the highest at the top surface.

(2) With increasing deformation temperature, the workability of the samples is improved, and fracture is less likely to occur. Sound products can be achieved after ECAP at 200 °C without CTC or even at 175 °C with CTC. This is attributed to (i) a reduction in the maximum principal stress at the top surface, (ii) a more uniform strain distribution throughout the sample, and (iii) an increase in the critical damage value in the C & L criterion with rising deformation temperature. The benefit from CTC is a reduction in deformation temperature by 25 °C and yet a sound product can be achieved.

(3) Lowering the deformation temperature by 25 °C is significant for the ECAP of the AZ31 alloy. It improves the cost-effectiveness of ECAP processing and also the mechanical properties of the ECAPed material as a result of a reduction in the fraction of recrystallized grains and an improvement in grain size uniformity.

Data availability

The raw data required to reproduce these findings are available to be requested from aeivani@iust.ac.ir. The processed data required to reproduce these findings are available to be requested from aeivani@iust.ac.ir.

Declaration of Competing Interest

I declare the authors have no competing interests as defined by Nature Research, or other interests that might be perceived to influence the interpretation of the article.

I declare the authors have no non-financial competing interests as defined by Nature Research, or other interests that might be perceived to influence the interpretation of the article.

REFERENCES

[1] Valiev R. Nanostructuring of metals by severe plastic deformation for advanced properties. Nat Mater 2004;3:511–6.

[2] Jafarian H, Eivani A. Texture development, and microstructure evolution in metastable austenitic steel processed by accumulative roll bonding and subsequent annealing. J Mater Sci 2014;49:6570–8.

[3] Jafarian HR, Anijdan SHM, Eivani AR, Park N. A comprehensive study of microstructure development and its corresponding tensile properties in nano/ultrafine-grained metastable austenitic steel during accumulative roll bonding (ARB). Mater Sci Eng 2017;703:196–204. https://doi.org/10.1016/j.msea.2017.07.050.

[4] Shadabroo MS, Eivani AR, Jafarian HR, Razavi SF, Zhou J. Optimization of inter-pass annealing for a minimum recrystallized grain size and further grain refinement towards nanostructured AA6063 during equal channel

angular pressing. Mater Char 2016;112:160–8. https://doi.org/10.1016/j.matchar.2015.12.018.
[5] Rahimi F, Eivani AR, Kiani M. Effect of die design parameters on the deformation behavior in pure shear extrusion. Mater Des 2015;83:144–53.
[6] Najafi S, Eivani AR, Samaee M, Jafarian HR, Zhou J. A comprehensive investigation of the strengthening effects of dislocations, texture and low and high angle grain boundaries in ultrafine grained AA6063 aluminum alloy. Mater Char 2018;136:60–8.
[7] Howeyze M, Eivani AR, Arabi H, Jafarian HR. Effects of deformation routes on the evolution of microstructure, texture and tensile properties of AA5052 aluminum alloy. Mater Sci Eng 2018;732:120–8.
[8] Valipour Sh, Eivani AR, Jafarian HR, Seyedein SH, Aboutalebi MR. Effect of pre-deformation thermomechanical processing on the development of ultrafine grain structure during equal channel angular extrusion. Mater Des 2016;89:377–84. https://doi.org/10.1016/j.matdes.2015.09.161.
[9] Kalahroudi FJ, Eivani AR, Jafarian HR, Amouri A, Gholizadeh R. Inhomogeneity in strain, microstructure and mechanical properties of AA1050 alloy during twist extrusion. Mater Sci Eng 2016;667:349–57. https://doi.org/10.1016/j.msea.2016.04.087.
[10] Mordike BL, Ebert T. Magnesium properties-application-potential. Mater Sci Eng 2001;302:37–45.
[11] Murty KL. Effect of c/a-ratio on crystallographic texture and mechanical anisotropy of hexagonal close packed metals. Mater Sci Forum 2003:3575–80.
[12] Staroselsky A, Anand L. A constitutive model for hcp materials deforming by slip and twinning: application to magnesium alloy AZ31B. Int J Plast 2003;19:1843–64. https://doi.org/10.1016/S0749-6419(03)00039-1.
[13] Wang YN, Huang JC. Texture analysis in hexagonal materials. Mater Chem Phys 2003;81:11–26. https://doi.org/10.1016/S0254-0584(03)00168-8.
[14] Goel NC, Cahoon JR. The Al-Li-Mg system (Aluminum-Lithium-Magnesium). Bull. Alloy Phase Diagr. 1990;11:528–46. https://doi.org/10.1007/BF02841712.
[15] Yamashita A, Horita Z, Langdon TG. Improving the mechanical properties of magnesium and a magnesium alloy through severe plastic deformation. Mater Sci Eng 2001;300:142–7. https://doi.org/10.1016/S0921-5093(00)01660-9.
[16] Sakai T, Belyakov A, Kaibyshev R, Miura H, Jonas JJ. Dynamic and post-dynamic recrystallization under hot, cold and severe plastic deformation conditions. Prog Mater Sci 2014;60:130–207. https://doi.org/10.1016/j.pmatsci.2013.09.002.
[17] Li X, Jiao F, Al-Samman T, Ghosh Chowdhury S. Influence of second-phase precipitates on the texture evolution of Mg–Al–Zn alloys during hot deformation. Scripta Mater 2012;66:159–62. https://doi.org/10.1016/j.scriptamat.2011.10.028.
[18] Gottstein G, Al Samman T. Texture development in pure Mg and Mg alloy AZ31. Mater Sci Forum 2005;623:495–7. https://doi.org/10.4028/www.scientific.net/MSF.
[19] Hosford WF, Caddell RM. Metal forming: mechanics and metallurgy. Cambridge University Press; 2011.
[20] Kang F, Wang JT, Peng Y. Deformation and fracture during equal channel angular pressing of AZ31 magnesium alloy. Mater Sci Eng 2008;487:68–73. https://doi.org/10.1016/j.msea.2007.09.063.
[21] Lapovok RYe. The role of back-pressure in equal channel angular extrusion. J Mater Sci 2005;40:341–6. https://doi.org/10.1007/s10853-005-6088-0.
[22] Figueiredo RB, Cetlin PR, Langdon TG. The processing of difficult-to-work alloys by ECAP with an emphasis on magnesium alloys. Acta Mater 2007;55:4769–79. https://doi.org/10.1016/j.actamat.2007.04.043.
[23] Valiev RZ, Estrin Y, Horita Z, Langdon TG, Zechetbauer MJ, Zhu YT. Producing bulk ultrafine-grained materials by severe plastic deformation. JOM (J Occup Med) 2006;58:33–9.
[24] Valiev RZ, Islamgaliev RK, Alexandrov IV. Bulk nanostructured materials from severe plastic deformation. Prog Mater Sci 2000;45:103–89.
[25] Humphreys FJ, Hatherly M. Recrystallization and related annealing phenomena. Elsevier; 2012.
[26] Xia K, Wang JT, Wu X, Chen G, Gurvan M. Equal channel angular pressing of magnesium alloy AZ31. Mater Sci Eng 2005;410–411:324–7. https://doi.org/10.1016/j.msea.2005.08.123.
[27] Xu C, Xia K, Langdon TG. Processing of a magnesium alloy by equal-channel angular pressing using a back-pressure. Mater Sci Eng 2009;527:205–11. https://doi.org/10.1016/j.msea.2009.07.063.
[28] Hu H, Zhang D, Pan F. Die structure optimization of equal channel angular extrusion for AZ31 magnesium alloy based on finite element method. Trans Nonferrous Metals Soc China 2010;20:259–66. https://doi.org/10.1016/S1003-6326(09)60132-1.
[29] Djavanroodi F, Omranpour B, Ebrahimi M, Sedighi M. Designing of ECAP parameters based on strain distribution uniformity. Prog. Nat. Sci. Mater. Int. 2012;22:452–60. https://doi.org/10.1016/j.pnsc.2012.08.001.
[30] Tork NB, Pardis N, Ebrahimi R. Investigation on the feasibility of room temperature plastic deformation of pure magnesium by simple shear extrusion process. Mater Sci Eng 2013;560:34–9. https://doi.org/10.1016/j.msea.2012.08.085.
[31] Djavanroodi F, Daneshtalab M, Ebrahimi M. A novel technique to increase strain distribution homogeneity for ECAPed materials. Mater Sci Eng 2012;535:115–21. https://doi.org/10.1016/j.msea.2011.12.050.
[32] Jahadi R, Sedighi M, Jahed H. Effects of aluminum and copper cover tube casing on the ECAP process of AM30 magnesium alloy. Mater Manuf Process 2017;32:1375–83. https://doi.org/10.1080/10426914.2016.1269917.
[33] Wierzbicki T, Bao Y, Lee Y-W, Bai Y. Calibration and evaluation of seven fracture models. Int J Mech Sci 2005;47:719–43. https://doi.org/10.1016/j.ijmecsci.2005.03.003.
[34] Cockcroft MG, Latham DJ. Ductility and the workability of metals. J Inst Met 1968;96:33–9.
[35] Mirghasemi SM, Eivani AR, Seyedein SH, Jafarian HR. A comparison between routine vs. normalized Cockroft-Latham fracture criteria for prediction of fracture during equal channel angular pressing. Eng Fract Mech 2018;199:721–9. https://doi.org/10.1016/j.engfracmech.2018.07.016.
[36] Yoon SC, Bok CH, Seo MH, Kim T-S, Kim HS. Comparison in deformation and fracture behavior of magnesium during equal channel angular pressing by experimental and numerical methods. Mater Trans 2008;49:963–6.
[37] Hamu GB, Eliezer D, Wagner L. The relation between severe plastic deformation microstructure and corrosion behavior of AZ31 magnesium alloy. J Alloys Compd 2009;468:222–9.
[38] Kim WJ, Jeong HG, Jeong HT. Achieving high strength and high ductility in magnesium alloys using severe plastic deformation combined with low-temperature aging. Scripta Mater 2009;61:1040–3.
[39] Kang SH, Lee YS, Lee JH. Effect of grain refinement of magnesium alloy AZ31 by severe plastic deformation on material characteristics. J Mater Process Technol 2008;201:436–40. https://doi.org/10.1016/j.jmatprotec.2007.11.305.

[40] Muralidhar A, Narendranath S, Shivananda Nayaka H. Effect of equal channel angular pressing on AZ31 wrought magnesium alloys. J. Magnes. Alloys. 2013;1:336–40. https://doi.org/10.1016/j.jma.2013.11.007.

[41] Li J, Li Z, Mao D, Zhang B, Chen S. Effect of annealing process on microstructure and properties of roll-casting AZ31B Mg alloy sheet. Procedia Eng 2012;27:895–902. https://doi.org/10.1016/j.proeng.2011.12.536.